

# Statistical Analysis of Close Approach Distances in the Geostationary Environment

Carl Toews and Eric Phelps

**ABSTRACT.** The Lincoln Laboratory predicts and monitors close approaches between certain commercial geostationary satellites and cataloged debris. Empirically generated histograms of closest approach distances consistently reveal a peak near 25km. This paper proposes an explanation based on the statistical distribution of debris ephemerides, extrapolating a simplified model for encounter geometry and using this model to suggest an approximate density function for close approaches.

## 1 Introduction

The Millstone Hill catalog of space debris presently contains approximately 10,000 objects. Of these, roughly 500 pose potential collision threats to active payload satellites in the geobelt. Lincoln Laboratory's Geosynchronous Monitoring and Warning System (GMWS) tracks many of these threat objects, monitoring their collision potential with a select set of active geosynchronous payloads by propagating the trajectories of both the payload and the drifter and issuing a warning if the predicted distance of closest approach (DCA) falls below some arbitrary upper bound. Empirically generated distributions of DCA consistently reveal a peak near 25 km (see Figure 1), and the question was posed as to why.

This paper attempts to answer this question by employing a statistical analysis of the debris ephemerides to explicitly write down a DCA density function. It does so by first considering orbital perturbations in the near geostationary environment in order to postulate inclination, eccentricity, and altitude distributions for the relevant debris population. It then uses these distributions and their consequences for encounter geometry to formulate an approximate three dimensional density function for close approaches. The density function is formulated for a payload-centric coordinate frame in which the  $x$ ,  $y$ , and  $z$  components correspond to the payload's radial, along, and cross tracks, respectively. Integration over shells of fixed radius then yields a density function for DCA. The central conclusion of the paper is that the position of the DCA peaks depends principally on the radial variance of the debris population.

The structure of the paper is as follows: Section 2 illustrates the pitfalls of an ill-chosen debris model by showing how applications of an existing model yield density functions very much at odds with empirical data. The roots of these differences are explored in Section 3, where a set of GMWS generated encounter statistics exposes the modeling problems of the previous section and suggests revisions based on encounter geometry. Section 4 justifies and develops these revisions, concluding with an analytic model connecting the DCA histogram to a certain confluent hypergeometric function. The last section discusses the limitations of this solution, and contains several suggestions for further research.

## 2 Preliminary Approaches

We begin by formalizing the problem and establishing some notation. Assume all orbiting objects can be represented as point particles, and take  $T$  to be the distance threshold below which a warning

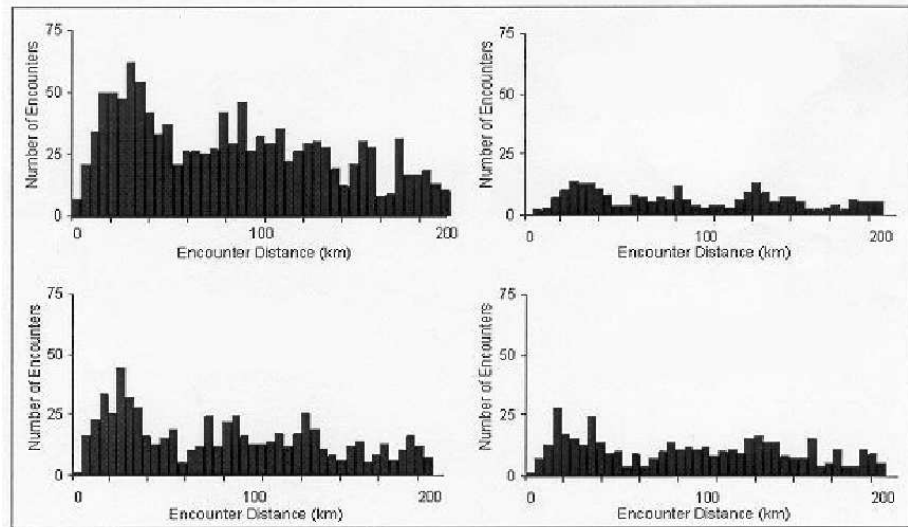


Figure 1: GMWS generated DCA histograms for 2001: each histogram displays total DCA for all satellites of a particular company.

is issued. Surround each payload by a spherical shell of radius  $T$ , and define an **encounter** as the time frame within which a debris particle is continuously contained in any such shell. For each encounter, let  $D$  denote the random variable corresponding to the distance of closest approach, and note that  $D$  can assume values between 0 and  $T$ . We are interested in the distribution of  $D$ .

Although we will be treating  $D$  as a random variable, it should be noted that it is not, for our purposes, modeling error or observational uncertainty that renders  $D$  stochastic, but rather the fact that values of  $D$  are generated by many encounters between many different orbiting objects. In particular, we are not interested in observationally conditioned close approach covariance, but rather in the average long term behavior of a physical process too complex to be deterministically described. Moreover, these averages may best be described by first identifying statistically homogeneous encounter classes and subsequently deriving different close approach distributions for each class. Some variant of this idea hovers in the background of the work in Section 4; however, when we speak of ‘the distribution of  $D$ ’, we will refer to the distribution of  $D$  averaged over the aggregate of all relevant debris objects.

In light of this comment, the starting point of our analysis must be a statistical representation of how this aggregate moves, as well as a model for how such motion determines the DCA histogram. One approach we considered was based on an idea developed in [1] for geostationary encounters and in [3] for general encounters. In both of these settings, the basic idea is to write down a spatial density function for debris and subsequently calculate collision rates by integrating this density over an appropriate volume. In [1], debris density is considered uniform over a toroidal region surrounding the geobelt, and the volume of integration is the volume swept out by the cross sectional area of the payload as it passes through this torus. Matters are complicated somewhat in [3], where debris is lumped into inclination dependent classes and the volume of integration is generated by an area perpendicular to the relative velocity vector. In both cases, debris density is considered isotropically uniform locally across the area generating the integration volume.

While well suited for certain kinds of collision analysis, this isotropic uniformity eliminates some of the statistical subtleties that surface when one considers relatively large surface areas, and as a consequence predicts a DCA histogram that increases monotonically with distance. There are various ways to see this, but one in harmony with the analysis in [1] might be as follows: a DCA of value  $d$  corresponds to a collision with every shell of radius between  $d$  and  $T$  but no shell smaller

than  $d$ . Accordingly, given two shells of respective radii  $d_1$  and  $d_2$ , the difference in the rate at which these shells generate collisions corresponds to the rate at which DCA's accrue in the range between  $d_1$  and  $d_2$ . Since the rate at which a shell of radius  $d$  generates collisions is proportional to its cross sectional area, we have

$$P(d_1 < D < d_2) = \int_{d_1}^{d_2} f(x) dx = \frac{1}{\pi T^2} (\pi d_2^2 - \pi d_1^2)$$

where  $f$  represents the density function of  $D$  and the factor on the left of the last line is a normalizing constant. Solving for the density function yields

$$f(x) = \frac{2}{T^2} x,$$

which suggests that the histogram of DCA should increase as a linear function of distance.

An analysis in accord with the ideas in [3] would proceed similarly for each debris class; the shape of the final histogram would then be determined by integrating over all such classes. Since the sum of monotonically increasing functions again increases monotonically, this approach too will lead to a monotonically increasing DCA histogram.

### 3 Analysis of GMWS Data

The modeling assumptions of the last section yielded monotonically increasing density functions, in contrast to the empirically based humped functions of Figure 1. To explain this disparity, we analyzed GMWS data for a set of 763 encounters between June 2002 and January 2003. The encounters were generated by 61 distinct debris objects and 34 distinct payloads. Most of the debris objects were geosynchronous satellites that had failed on orbit and begun to drift; launch dates were fairly evenly scattered over the last 35 years. The data for each encounter included the radial, cross, and along track components of the point of closest approach (expressed relative to the payload), as well as element sets for both the debris object and the payload. Since GMWS produces multiple predictions for each close approach, the statistics for each encounter were taken from the prediction immediately preceding the conjunction.

Figure 2 shows the positional distribution of the encounters, broken down into components. The first thing to note is the highly non-uniform nature of the data. If closest approach points were distributed uniformly within a ball, one would expect any cross section to consist of points uniformly filling a circle. Instead, only the radial vs. along track distribution even remotely approaches this pattern: most tellingly, the cross vs. along track distribution shows a definite double-cone type structure, a distribution that in turn determines the flat-pancake look for the radial vs. cross track distribution.

Histograms of the radial, cross, and along track distributions are shown in Figure 3. Again, if the points of closest approach were volumetrically uniform, one would expect all three of these histograms to be bell-shaped, with a peak at 0 and tails touching the  $x$ -axis at  $T$  and  $-T$ . Instead, the along track histogram is almost uniform, slightly weighted toward the positive scale, and the cross track histogram is sharply constrained around the origin. Only the radial distribution begins to approach the bell shaped ideal.

Distributions of eccentricity, inclination, and semi-major axis are illustrated in Figure 4. The eccentricities are all small and approximately Rayleigh distributed with parameter  $\sigma = 9 \times 10^{-8}$ . The semi-major axes cluster tightly around the nominal geostationary radius of 42165 km, reflecting the relative absence of non-conservative forces in the geostationary environment. Finally, the inclinations are approximately uniformly distributed between 0 and 15 degrees.

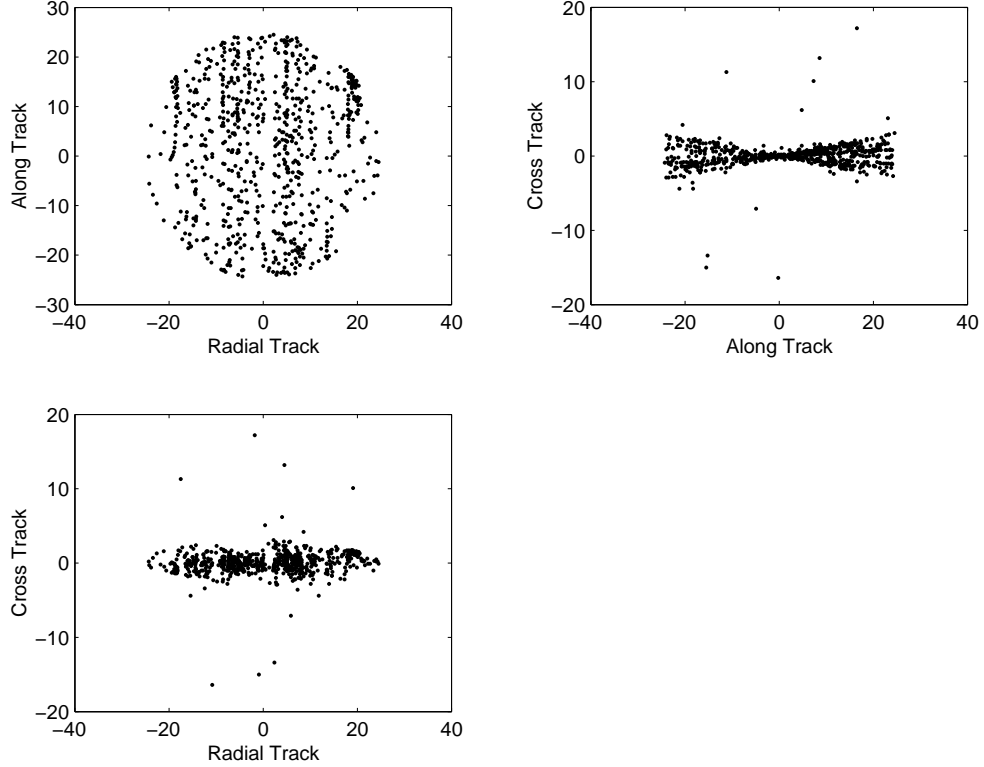


Figure 2: Encounter Cross Sections

## 4 Revised Model

### 4.1 Eccentricity Issues

Recall that the Rayleigh density is given by

$$p(x) = \frac{x}{\tau} \cdot \exp(-x^2/2\tau), \quad (1)$$

where  $x \geq 0$  and  $\tau$  is a positive parameter. We have observed that the eccentricity of the debris population essentially satisfies a Rayleigh distribution with parameter  $\tau = 9 \times 10^{-8}$ . Although for our purposes this distribution will be taken as a starting point, it is instructive to consider how one might develop a statistical model for such a density function.

The debris we are considering consists primarily of defunct geostationary satellites that have begun to drift. While active, each such satellite maintained a nominal null eccentricity, with permissible deviations determined by station keeping requirements. As discussed in [4], solar radiation pressure dominates subsequent secular evolution, with the eccentricity vector  $\mathbf{e} = (e_x, e_y)$  annually tracing a circle of radius

$$R_e \cong 10^{-2} \frac{C_p S}{M},$$

where  $C_p$  is the reflectivity coefficient of the satellite (usually close to 1.5), and  $S/M$  is the effective area to mass ratio (close to .02). Substituting numeric values for  $C_p$  and  $S/M$  gives an approximate radius of  $3 \times 10^{-4}$ ; allowing one radius of initial displacement and two radii of evolutionary displacement suggests that we can expect the magnitudes of  $e_x$  and  $e_y$  to be dispersed between 0 and  $3R_e$ . If we now consider  $e_x$  and  $e_y$  independent and identically distributed zero-mean Gaussians, we can

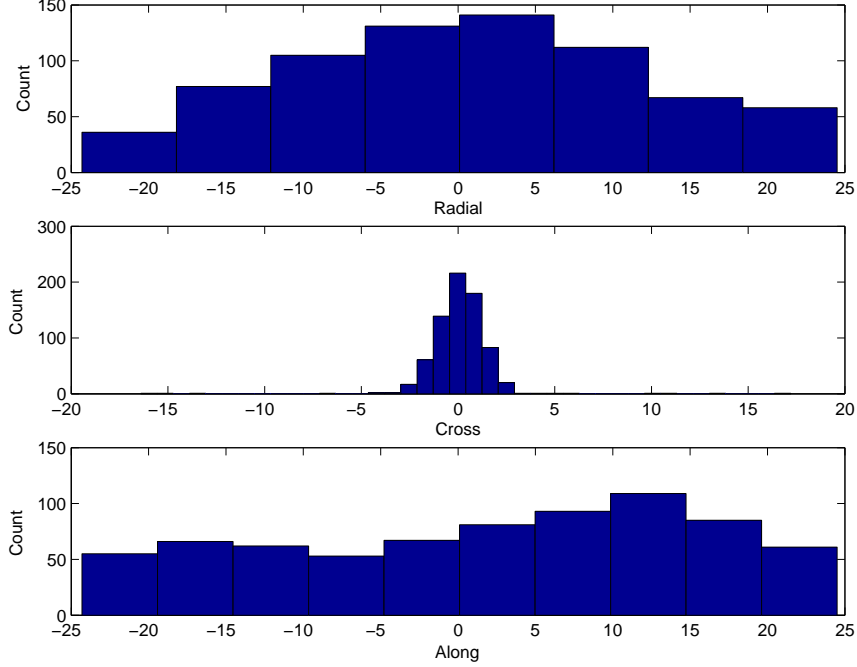


Figure 3: Component Distributions

approximate their common variance by setting the upper bound of their magnitudes equal to three standard deviations, i.e. setting the standard deviation equal to  $R_e$ . Finally, recall that if  $X$  and  $Y$  are independent identically distributed Gaussians with zero mean and  $\tau$  variance, then the random variable  $Z = \sqrt{X^2 + Y^2}$  is distributed Rayleigh with parameter  $\tau$ . Since the standard deviation of  $e_x$  and  $e_y$  is assumed to be  $R_e$ , our tentative model suggests that the eccentricity magnitude  $|e|$  will be Rayleigh distributed with parameter  $R_e^2 = 9 \times 10^{-8}$ .

## 4.2 Radial Issues

It is shown in [2] that if time is taken as random, the radial density function for an elliptic orbit with eccentricity  $e$  can be expressed as

$$p(r|e) = \frac{1}{\pi a^2} \frac{r}{(e^2 - c^2)^{1/2}}, \quad (2)$$

where

$$c = \frac{r - a}{a}.$$

By (1) and the discussion of Section 4.1, the eccentricity distribution satisfies

$$p(e) = \frac{e}{\tau} \cdot \exp(-e^2/2\tau), \quad \tau = 9 \times 10^{-8}. \quad (3)$$

Combining (2) with (3) yields

$$\begin{aligned} p(r) &= \int_e p(r|e)p(e)de \\ &= \frac{r}{\pi a^2 \tau} \int_c^1 \frac{e \cdot \exp(-e^2/2\tau)}{(e^2 - c^2)^{1/2}} de \end{aligned}$$

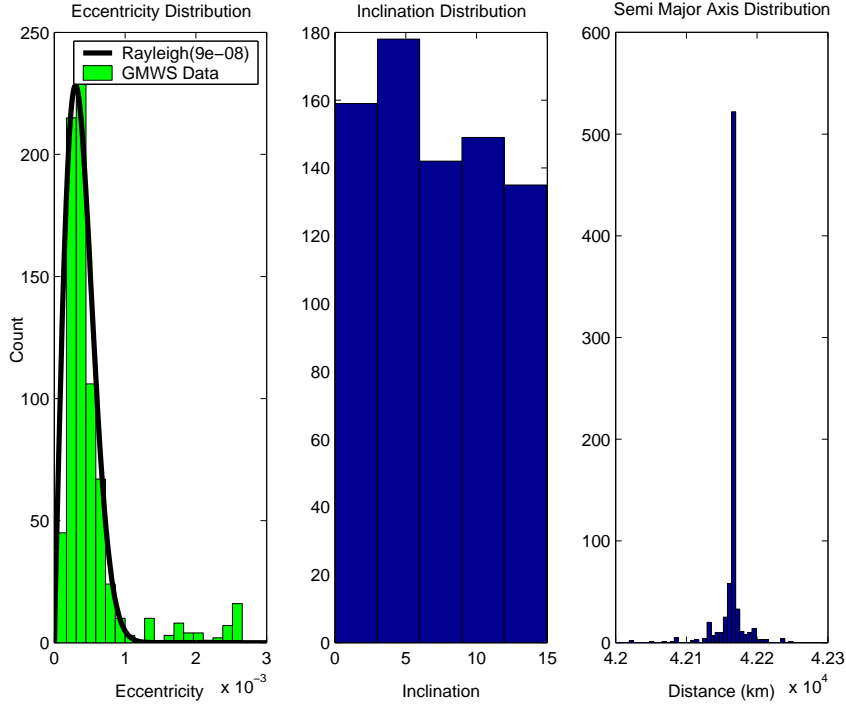


Figure 4: Debris Element Set Distributions

One can show that this integral solves as

$$p(r) = \frac{r}{a^2 \sqrt{2\pi\tau}} \cdot e^{-c^2/2\tau} \operatorname{erf} \left( \sqrt{\frac{1-c^2}{2\tau}} \right),$$

which can be expressed in terms of  $c$  as

$$p(c) = \frac{(c+1)}{\sqrt{2\pi\tau}} \cdot e^{-c^2/2\tau} \operatorname{erf} \left( \sqrt{\frac{1-c^2}{2\tau}} \right).$$

Although this result may be interesting in its own right, a more useful approximation can be had by observing that as  $\tau \rightarrow 0$ , the function  $p(c)$  approaches a Gaussian with mean 0 and variance  $\sqrt{\tau}$ . This approximation is quite good for the very small  $\tau$  characterizing the Rayleigh distribution of the eccentricities. Since  $r = a(c+1)$ , it follows that

$$p(r) \cong N(a, \sigma), \tag{4}$$

where  $\sigma = a\sqrt{\tau}$ . For nominal values  $a = 42165$  and  $\tau = 9 \times 10^{-8}$ , the standard deviation  $\sigma$  is approximately 13 km.

### 4.3 Inclination Issues

The distribution of inclinations is easily explained by considering the scattering of launch dates and the well known long term cyclic inclination evolution of geosynchronous drifters. In particular, random launch dates suggests random failure dates, and since the inclination of each failed satellite will evolve up to 15 degrees and back again in roughly 54 years, a random dispersion between these bounds can be expected.

For our purposes, the real interest of the inclination distribution lies in its connection to Figure 2. A closer inspection of the GMWS data reveals a roughly one-to-one correspondence between a debris particle's inclination and the magnitude of the cross to along track ratios at its points of closest approach. In particular, these ratios are all approximately  $i/2$ , where  $i$  is the inclination of the debris object in radians. When  $i$  is at its maximum value of  $15^\circ$ , this ratio is approximately .13, a value that corresponds quite well to the slope around the double cone structure in Figure 2.

Although this relation is really a simple and intuitive consequence of the fact that the relative position vector must be perpendicular to the relative velocity vector at the time of an encounter, for the sake of completion we sketch a derivation: define a payload-centric coordinate system with the positive  $y$ -axis directed along the payload's velocity vector, the positive  $x$ -axis lying in the equatorial plane and pointing away from the earth, and the  $z$ -axis chosen to render the system right handed. The idealized velocity vector of the payload can be written in this coordinate system as

$$\mathbf{v}_p = v(0, 1, 0) \quad (5)$$

where  $v$  denotes the idealized speed of a geosynchronous satellite. Suppose the debris particle orbits in a plane inclined at an angle  $i$  from the equatorial plane, and let  $L$  represent the ray originating from the center of the earth and passing through the ascending node of the debris particle. Writing the velocity vector of the debris object as  $\mathbf{v}_d = v_d \mathbf{e}_d$ , it is not hard to show that the unit vector  $\mathbf{e}_d$  can be expressed as

$$\mathbf{e}_d = R_{-\theta_p} R_i R_{\theta_d} R_\gamma \mathbf{e}_p,$$

where  $R_{-\theta_p}$ ,  $R_{\theta_d}$ , and  $R_\gamma$  represent rotations in the  $x, y$ -plane through angles  $-\theta_p$ ,  $\theta_d$ , and  $\gamma$ , respectively, while  $R_i$  represents a rotation around the  $x$ -axis by an angle  $i$ . The variables  $\theta_p$  and  $\theta_d$  denote the angles formed by  $L$  and the position vectors of the payload and the debris particles, respectively, while  $i$  and  $\gamma$  denote debris inclination and flight path angle; without loss of generality, we may assume that  $i$  is between 0 and  $15^\circ$ ,  $\gamma$  is between 0 and  $\pi/2$ , and,  $\theta_p$  and  $\theta_d$  lie in the range  $[-\pi/2, \pi/2]$ . (Note that this formulation implicitly assumes that both the payload and the debris are orbiting in the same general direction.) Writing out the rotation matrices explicitly, one can show that

$$\mathbf{v}_d = (v + v_\epsilon) \cdot (a, b, c),$$

where

$$\begin{aligned} a &= -\cos(\theta_p) \sin(\theta_d - \gamma) + \sin(\theta_p) \cos(i) \cos(\theta_d - \gamma) \\ b &= \sin(\theta_p) \sin(\theta_d - \gamma) + \cos(\theta_p) \cos(i) \cos(\theta_d - \gamma) \\ c &= \sin(i) \cos(\theta_d - \gamma). \end{aligned}$$

The quantity  $v_\epsilon$  represents the deviation from the idealized payload speed  $v$ . Possible values for  $v_\epsilon$  depend on the orbital energy and eccentricity of the debris object, but for the objects considered here,  $v_\epsilon \ll v$ . Similarly, it is not hard to show that for a moderate inclination and a moderate threshold parameter  $T$  (e.g.  $i > 1^\circ$  and  $T < 200$ ), the angles  $\theta_p$ ,  $\theta_d$ , and  $\gamma$  at the time of an encounter are all much smaller than  $i$ . Accordingly, a good first order approximation to the velocity of the debris vector can be obtained by setting  $v_\epsilon$ ,  $\theta_p$ ,  $\theta_d$  and  $\gamma$  all equal to zero. The approximate relative velocity of the two objects near the time of the encounter is thus

$$\mathbf{v}_{\text{rel}} = \mathbf{v}_d - \mathbf{v}_p \cong v(0, \cos i - 1, \sin i). \quad (6)$$

Finally, note that since position is a smooth function of time, the relative position  $\mathbf{r}_{\text{rel}}$  at the time of an encounter must satisfy

$$\mathbf{r}_{\text{rel}} \cdot \mathbf{v}_{\text{rel}} = 0, \quad (7)$$

Combining (6) with (7) shows that the point of closest approach between the payload and a debris object of inclination  $i$  will satisfy

$$\left| \frac{\text{cross}}{\text{along}} \right| \cong \frac{1 - \cos i}{\sin i} = \frac{\sin i}{1 + \cos i} \cong \frac{i}{2}. \quad (8)$$

Equation (8) states the basic relation between the along to cross track ratio of the encounter coordinates and the inclination angle of the debris. It must be emphasized that the relation is only approximate (although the approximation improves with increasing inclination): indeed, whenever the relative velocity vector has *any* component in the radial direction, the surface defined by its complement includes points for which this ratio is arbitrary. A more sophisticated analysis would probabilize the point where the debris punctures a skewed surface and use this to derive a probability density for the along to cross track ratio. Our simplified approach degenerates for very small values of  $i$ , as evidenced by the few points in the upper right plot of Figure 2 that lie randomly scattered outside the double cone structure.

#### 4.4 An Approximate Analytic Solution

In what follows,  $C$  represents a constant whose value may change from line to line but which is always independent of the variables of integration. The symbol  $\sim$  will indicate proportionality.

Let  $P = (x, y, z)$  represent the point of closest approach, where  $x$ ,  $y$  and  $z$  correspond, as usual, to the payload's radial, along, and cross track dimensions, respectively. We would like to write an approximate local density function for  $P$  based on the calculations of the last three subsections.

The expression for the relative velocity given in (6) shows that  $x$  depends only on the radial component of the drifter at the time of the encounter; in particular, it is independent of both  $y$  and  $z$ , and if encounter time is assumed random, its distribution mirrors that of the general population given in (4), i.e.

$$p(x) \sim \frac{1}{\sqrt{2\pi\sigma^2}} e^{-x^2/2\sigma^2}, \quad (9)$$

where  $\sigma \cong 13\text{km}$ .

The along track component  $y$  depends on relative positions of the payload and the drifter within their respective orbits. If we assume, as in [3], that ascending nodes for any inclination class are uniformly distributed and that, for a given orbital plane, the orbital phase is uniform, we are led to model the along track as uniform as well, i.e.

$$p(y) \sim 1. \quad (10)$$

The cross track component  $z$  is uniquely determined by  $y$  and the inclination of the drifter. If we assume that  $y$  and  $i$  are independent and that  $i$  is uniformly distributed between 0 and  $I = 15^\circ$ , then the approximation  $|z/y| = i/2$  given in (8) can be used to write down a conditional density for  $z$ :

$$p(z|y) \sim \frac{\chi_y(z)}{y}, \quad (11)$$

where  $\chi_y(z)$  denotes the characteristic function of the interval  $[-Iy/2, Iy/2]$ , defined by

$$\chi_y(z) = \begin{cases} 1 & z \in [-Iy/2, Iy/2] \\ 0 & \text{otherwise} \end{cases}$$

Finally, combining (9), (10), and (11) with the relation

$$p(x, y, z) = p(x|z \cap y)p(z|y)p(y)$$

and using the assumption that  $p(x|z \cap y) = p(x)$ , we see that an approximate density function for close approach distances is given by

$$p(x, y, z) = C \cdot \frac{e^{-x^2/2\sigma^2}}{y} \cdot \chi_y(z),$$

where  $C$  is a normalizing constant that will depend on the shape and size of the encounter region. Converting to spherical coordinates yields:

$$p(r, \theta, \lambda) = C \cdot \frac{r e^{-r^2 \cos^2 \lambda \cos^2 \theta / 2\sigma^2}}{\sin \theta} \cdot \chi_\theta(\lambda),$$

where

$$\chi_\theta(\lambda) = \begin{cases} 1 & |\lambda| < \tan^{-1}(I |\sin \theta| / 2) \\ 0 & \text{otherwise.} \end{cases}$$

The density function  $p(r)$  can be derived from this expression by fixing  $d$  and integrating over the encounter region with respect to  $\theta$  and  $\lambda$ . In particular, if we consider a spherical encounter region and temporarily ignore the constant, we get

$$p(r) = 8 \int_0^{\pi/2} \int_0^{\tan^{-1}(I \sin \theta / 2)} \frac{r e^{-r^2 \cos^2 \lambda \cos^2 \theta / 2\sigma^2}}{\sin \theta} d\lambda d\theta, \quad (12)$$

where we use the symmetry of the encounter region to restrict  $\theta$  to the interval  $[0, \pi/2]$  and to consider only positive  $\lambda$ .

Although this integral as such is rather intractable, it can be approximated by noting that since  $\lambda < I = 15^0$ ,

$$\cos^2 \lambda \cong 1 \quad (13)$$

and

$$\tan^{-1}(I/2 * \sin \theta) \cong I/2 * \sin \theta. \quad (14)$$

For the sake of argumentative continuity, we postpone for the moment a discussion of the errors introduced by these approximations and continue with the main thread of the argument: substituting (13) and (14) into (12) and simplifying yields:

$$p(r) = C \int_0^{\pi/2} r e^{-r^2 \cos^2 \theta / 2\sigma^2} d\theta,$$

where we now subsume all constant terms, including a normalizing factor, into the symbol  $C$ . This integral admits an analytic solution of the form

$$p(r) = C \cdot r M\left(\frac{1}{2}, 1, \frac{-r^2}{2\sigma^2}\right), \quad (15)$$

where  $M(a, b, z)$  is the confluent hypergeometric function with parameters  $a$  and  $b$ . The function  $M(a, b, z)$  satisfies the differential equation

$$z \frac{d^2 w}{dz^2} + (b - z) \frac{dw}{dz} - aw = 0, \quad (16)$$

and can be represented in series as

$$M(a, b, z) = 1 + \frac{az}{b} + \frac{(a)_2 z^2}{(b)_2 2!} + \dots + \frac{(a)_n z^n}{(b)_n n!} + \dots \quad (17)$$

where

$$(a)_n = a(a+1)(a+2)\dots(a+n-1), \quad (a)_0 = 1.$$

A plot of (15) is shown in Figure (5). To calculate the position of the hump, we use (16) and (17) to differentiate (15) with respect to  $r$ , yielding

$$p'(r) \sim M\left(\frac{1}{2}, 1, z\right) - z M\left(\frac{3}{2}, 2, z\right) \quad (18)$$

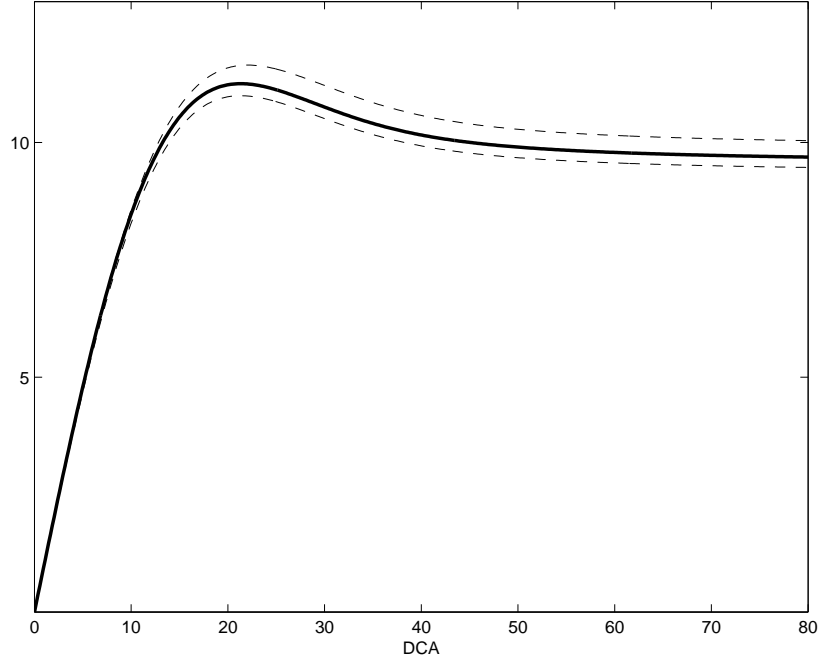


Figure 5: Analytic solution to Close Approach Histogram (the y-axis is a linear scale).

where

$$z = \frac{r^2}{2\sigma^2}.$$

Equation (18) has a root at  $z_0 \cong 1.6$ . It follows that the peak of the DCA histogram will be at

$$r_0 = \sqrt{2(1.6)} * \sigma.$$

We have suggested that  $\sigma \cong 13$ . For this value,  $r_0 \cong 23$ , which corresponds quite well to the empirical hump.

Lastly, a note on errors: set  $x = I/2 * \sin \theta$ , and employ elementary calculus to show that since  $|x| \in [0, I/2]$  with  $I = 15^0$ ,

$$\tan^{-1}(x) > .99x.$$

Also note that the integrand of (12) decreases monotonically as  $\cos \lambda$  increases. An upper bound for the solution can be obtained by setting  $\cos \lambda = \cos 15 = .965$  and integrating from 0 to  $I/2 * \sin \theta$ ; a lower bound can be obtained by setting  $\cos \lambda = 1$  and integrating from 0 to  $(.99) * I/2 * \sin \theta$ . The corresponding envelope is pictured in Figure 5, and reveals that the error is negligible.

## 5 Conclusions and Caveats

The central conclusion of this paper is that the position of the peak of the DCA histogram depends primarily on the radial variance of the drifter population and is independent of the threshold parameter  $T$ . This result presupposes a Gaussian radial distribution, a uniform along track distribution, and an inclination distribution that is uniform within appropriate bounds.

The central caveat of this paper is that the above distribution assumptions are only approximate, and that the true distributions will evolve in time. Indeed, although the analytic solution of the last section succeeds rather well in recapturing the general form of empirical DCA histograms, the result

is subject to several limitations. Firstly, the assumption of a perfectly uniform along track density loses some credibility in the face of histograms such as the bottom plot of Figure 3, which shows a slight shift in the positive direction. Numerical simulations based on the propagation of the existing data set reproduce this shift, for reasons we do not fully understand. Secondly, the assumption that the cross track component depends uniquely on inclination and along track breaks down in the case of very low inclination drifters; a more comprehensive model would refine its consideration of this subpopulation. Similarly, the assumption of small angles  $\theta_a$  and  $\theta_p$  in Section 4.3 presupposes a relatively small DCA threshold  $T$ ; accordingly, the predictions of the last section cannot be expected to hold as  $T$  increases without bound. Finally, the various distributional assumptions can certainly be refined: account might be taken of semi-major axis evolution, and the inclination model could better attempt to capture patterns of drift and failure.

## References

- [1] R. LeClair, R. Sridharan, *Probability of Collision In the Geostationary Orbit*, Third European Conference on Space Debris. Vol. 1, Darmstadt, Germany, Mar. 19-21, 2001, Noordwijk, Netherlands, European Space Agency, 2001, p. 463-470
- [2] K.C. Carlton-Wippern, *Statistical Analysis of Elliptical Keplerian Orbits, With Applications to Search and Surveillance Algorithms*, Space Power - Resources, Manufacturing and Development , vol. 9, no. 4, 1990, p. 349-364.
- [3] K. Chan, *Close Encounters With Multiple Satellites*, Spaceflight Mechanics 2002; Proceedings of the AAS/AIAA Space Flight Mechanics Meeting. Vol. 1, San Antonio, TX, Jan. 27-30, 2002, San Diego, CA, Univelt, Incorporated, 2002, p. 281-300.
- [4] G. Campan, F. Alby, H. Gautier, *Station-Keeping Techniques for Geostationary Satellites*, Spaceflight dynamics. Pt. 2 (A95-45701 12-13), Toulouse, France, Cepadues-Editions, 1995, p. 979-1081.